Spectroscopic Calibration of Modern Density Functional Methods Using $[CuCl_4]^{2-}$

Robert K. Szilagyi, Markus Metz, and Edward I. Solomon*

Department of Chemistry, Stanford University, 333 Campus Dr., Stanford, California 94305

Received: November 9, 2001

Density functional theory has become a popular method for studying the electronic structure and potential energy surface properties of large molecules. Its accuracy has been extensively validated for organic and organometallic systems. However, this is not yet the case for classical inorganic compounds with biological importance. This study presents a systematic evaluation of modern DFT calculations using the spectroscopically well understood molecule $[CuCl_4]^{2-}$. The BP86 and B3LYP functionals with saturated basis sets give a ground-state bonding description that is too covalent, and the calculated ligand-field and ligand-to-metal charge transitions are shifted to higher and lower energies, respectively, relative to experiment. A spectroscopically adjusted hybrid DFT functional (B(38HF)P86) was optimized to match the ground-state experimental Cu spin density (0.62 ± 0.02e). This adjusted hybrid functional also gives an improved excited-state description with a rms error in transition energies of 1000 cm^{-1}. The potential energy surface of the $[CuCl_4]^{2-}$ was studied in gas and condensed phases. In the gas phase, the tetragonal (D_{4h}) geometry was found to be a transition state along the b_{2u} distortion mode connecting distorted tetrahedral (D_{2d}) structures. The replacement of 38% local + nonlocal DF exchange with HF exchange improves the calculated Cu−Cl bond lengths by 0.03 Å, increases the frequency of the a_{1g} mode by 30 cm^{-1} and changes the energetics by 3 kcal mol^{-1} relative to the BP86 method. It is found that the crystal lattice stabilizes the D_{4h} $[CuCl_4]^{2-}$ structure through van der Waals and hydrogen bonding interactions worth about 10 kcal mol^{-1} demonstrating the role of the environment in determining the geometric and electronic structure of the Cu site. The importance of the type and the amount of DF correlation has been investigated and alternative nonhybrid methods of adjusting the ground-state description have been evaluated.

1. Introduction

Density functional theory[1] is extensively used in many areas of chemistry in particular, in bioinorganic chemistry,[2−4] where the complexity of the active site models requires large-scale calculations not yet accessible at high level ab initio theory. Two approaches (the BP86[5,6] and B3LYP[7] sets of functionals) are generally utilized and are having significant impact on our understanding of intermediate and transition state structures and the relative energies of chemical processes. The BP86 set of functionals was one of the first gradient corrected (GGA) DFT methods found to be more accurate than the early local density approximations.[8] Further improvement in DFT theory was achieved with the introduction of hybrid functionals, such as B3LYP. These were developed to fit atomization and ionization energies and proton affinities of small organic molecules (the so-called Gaussian-1 set[9,10]) with average precision of 2 kcal mol^{-1}.

The purpose of this study is to apply these GGA and hybrid DFT methods to a simple inorganic metal complex to evaluate how well these functionals perform relative to experiment. For transition metal containing systems, thermochemical data are rare, and when available, their accuracy can be questionable. Therefore, we calibrate the DFT methods using spectroscopic properties including spin densities and transition energies.

A considerable amount of ground and excited-state experimental data are available for the tetragonal (D_{4h}) and tetrahedral (D_{2d}) $[CuCl_4]^{2-}$ complexes. A selected data set[11,12] is summarized in Table 1, which can be directly compared with the results from electronic structure calculations. The highest antibonding orbital in this d^9 system defines the ground-state spin density of the Cu ion in the D_{4h} structure as $62 \pm 2\%$. Due to the reliability of these experimental data, the $[CuCl_4]^{2-}$ system was selected to evaluate the DFT calculations.

TABLE 1: Experimentally Determined HOMO d-Orbital Character (in percent) for $[CuCl_4]^{2-}$

method	D_{4h}	D_{2d}
g-values − EPR, adjusted Xα-SW	61	71
copper hyperfine − EPR	67	69
chloride superhyperfine − EPR	64	75
LF and CT energies − CI model	56	63
core level excitations − XPS satellite	60	68
valence level excitations − variable energy photoemission	65	68

This study has impact beyond the cupric chloride model system. Historically, the ground-state description of the Blue Cu protein active site was developed based on the electronic structure of the tetragonal $[CuCl_4]^{2-}$ complex.[13−15] The bridge between experiment and theory was provided by early Xα scattered wave (Xα-SW) calculations,[16−19] which were found to be too covalent for both systems.[20,21] After adjusting the Xα atomic sphere parameters to fit the $[CuCl_4]^{2-}$ experimental data, the calculated ground-state description was in good agreement with experiment for these and many other Cu(II) containing systems.

A similar approach is presented here to evaluate the accuracy of the electronic structure for the ground and excited-states calculated by BP86 and B3LYP functionals. As in the case of the nonadjusted Xα-SW method, we find that these standard

* To whom correspondence should be addressed. E-mail: Edward.Solomon@Stanford.EDU. Fax: +1 650 725−0259.

10.1021/jp014121c CCC: $22.00
Published on Web 02/27/2002

TABLE 2: List of Basis Sets Employed in the Study

Gaussian-type all electron basis sets (GTO)						
symbol		description		contraction scheme	pol. funct. (coefficient)	ref
BS1	Cu:	STO-3G	(12s9p3d)	333/333/3		99
	Cl:		(9s6p)	333/33		
BS2	Cu:	3-21G	(12s9p3d)	33321/3321/21		100,101
	Cl:		(9s6p)	3321/321		
BS3	Cu:	6-31G*	(22s16p4d)	66631/6631/31	f 0.80	91,102
	Cl:		(16s10p)	6631/631	d 0.75	
BS4	Cu:	6-311G	(14s9p6d)	61111111/51111/311	d 0.75	103,104
	Cl:	6-31G*	(16s10p)	6631/631		
BS5	Cu:	VTZ*	(14s9p6d)	62111111/33111/311	p 0.17 d0.13 f0.39	105
	Cl:	6-31G*	(16s10p)	6631/631	d 0.75	
BS6	Cu:	TZV*	(17s10p6d)	842111/631/411	f 0.48,0.14,0.43	106
	Cl:		(14s9p)	73211/6111	d 3.0,0.75,0.19	

Slater-type all electron basis sets (STO)[107]					
symbol		description		definition	pol. funct. (coefficient)
BSI	Cu:	single-ζ w/o	(4s3p1d)	ζ 1−4s 2−4p 3d	
	Cl:	polarization	(3s2p)	ζ 1−3s 2−3p	
BSII	Cu:	double-ζ and triple-	(8s5p3d)	ζ 4p ζζ 1−4s 2−3p ζζζ 3d	
	Cl:	ζ for 3d set	(6s4p)	ζζ 1−3s 2−3p	
BSIII	Cu:	see BSIV	(9s5p3d)	ζ 4p ζζ 1−3s 2−3p ζζζ 3d 4s	
	Cl:	BSII w/pol.func.	(6s4p1d)	ζ 3d ζζ 1−3s 2−3p	d (2.00)
BSIV	Cu:	triple-ζ w/o	(9s5p3d)	ζ 4p ζζ 1−3s 2−3p ζζζ 3d 4s	
	Cl:	polarization	(7s5p)	ζζ 1−2s 2p ζζζ 3s 3p	
BSV	Cu:	see BSIV	(9s5p3d)	ζ 4p ζζ 1−3s 2−3p ζζζ 3d 4s	
	Cl:	triple-ζ w/pol.func.	(7s5p1d1f)	ζ 3d 4f ζζ 1−2s 2p ζζζ 3s 3p	d (2.00) f (2.00)

effective core potentials and valence electron basis sets (ECP)						
symbol		description		contraction scheme	pol. funct. (coefficient)	ref
ECP1	Cu:	LANL1MB	(3s2p5d)	3/2/5		92,93
	Cl:		(3s3p)	3/3		
ECP2	Cu:	LANL2DZ	(8s5p5d)	341/311/41		94
	Cl:		(3s3p)	21/21		
ECP3	Cu:	LANL2DZ	(8s5p5d)	341/311/41	d 0.75	94,102
	Cl:	6-31G*	(16s10p)	6631/631		
ECP4	Cu:	CEP-121G	(9s9p6d)	4211/4211/411		108,109
	Cl:		(4s4p)	121/121		
ECP5	Cu:	SDD	(8s7p6d)	311111/22111/411		72,74,75,110−112
	Cl:		(12s8p)	531111/4211		
ECP6	Cu:	SDD*	(8s7p6d)	311111/22111/411	f 0.80	
	Cl:		(12s8p)	531111/4211	d 0.75	

DFT methods give a ground-state bonding description which is too covalent for cupric complexes. The hybrid density functional approach of Becke[7,22,23] is then used to adjust the ground-state atomic spin density to experiment. The effects of the new functional on the properties of the potential energy surface are systematically investigated. A proper calibration will allow the study of reaction coordinates and characterization of experimentally nonobservable species with predictive accuracy.

To probe the effect of the environment, both vacuum and solid state calculations have been performed. As considered previously, we find that the role of the environment is crucial. The stability of the planar geometry can be achieved only by proper modeling of lattice effects regardless of the level of theory. We find that in vacuum, the D_{4h} geometry is a saddle point with one imaginary frequency corresponding to a b_{2u} distortion which cannot be eliminated by the simple point charge models suggested earlier.[24−26]

In addition to defining an experimentally adjusted hybrid density functional, this study assesses the importance of the type and the amount of DF correlation functional. The performance of DF correlation is also compared with the results of selected wave function based methods. Alternative approaches are considered for software packages where the hybrid method is not accessible. The relevance of our study to the electronic and geometric structures of biological cupric active sites is discussed.

2. Methods and Details of Computations

The experimental structures for D_{4h} and D_{2d} $[CuCl_4]^{2-}$ complexes were taken from the crystal structure of $((C_6H_5)CH_2CH_2NH(CH_3)H)_2[CuCl_4]^{2-}$,[27] abbreviated as $(nmpH)_2CuCl_4$. Due to asymmetric solid-state interactions from the lattice,[28] the Cu−Cl bond lengths in planar and tetrahedral geometries slightly differ from each other (2.248 and 2.281 Å in D_{4h}, 2.190 and 2.227 Å in D_{2d}); however, the bond and dihedral angles are very close to their ideal values (see further discussion in 3.4.2). In this paper, the average values 2.264 and 2.208 Å were used. No gas-phase structural or thermochemical data have been found in the literature, therefore where applicable, the DFT results were related to high level ab initio calculations.

Density functional calculations were performed using Amsterdam Density Functional 2000.01[29−32] and Gaussian98[33] packages. In these calculations, we have used a wide variety of Gaussian- and Slater-type bases as summarized in Table 2, with five d- and seven f-type functions. In addition to the all-electron basis sets, various effective core potentials were evaluated.

SCHEME 1: Conceptual Relationship among GGA, Hybrid Density Functional and Hartree−Fock Theory

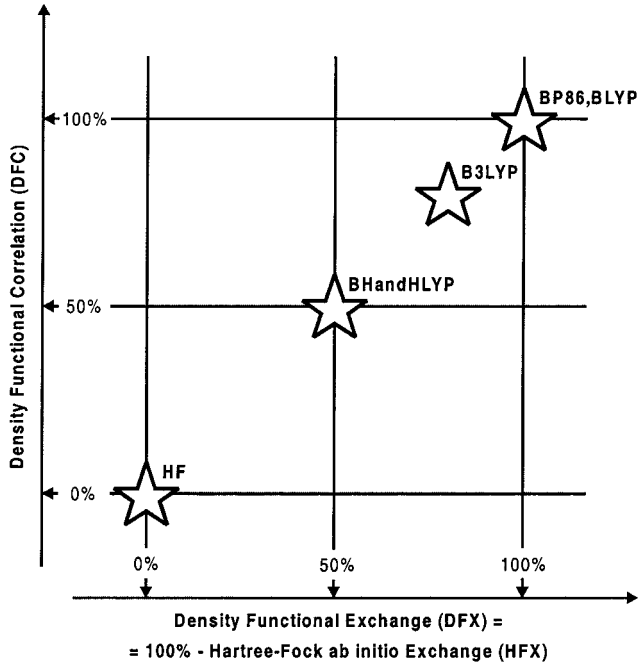

The adjustment of the amount and type of density functional exchange (DFX) and correlation (DFC) were conveniently achieved using the IOp keywords of the Gaussian98 program. The options 46, 47, and 45 of Overlay 5 were utilized to construct the density functionals from local and nonlocal DF exchange, local and nonlocal DF correlation and HF exchange, respectively. In this study, the Slater-type local density approximation[8,34,35] was used, supplemented with the Becke 1988 GGA functional[6] (B88) to define the total DF exchange. The Perdew 1986[5] (P86) and Lee−Yang−Parr (LYP) nonlocal DF correlations[36,37] were employed with Perdew 1981[38] (P81) and Vosko−Wilk−Nussair[39] (VWN) local DF correlation functionals, respectively. Among the well-defined hybrid functionals, Becke's 3-parameter[7] with LYP (B3LYP) and P86 (BP86) correlation functionals and Becke's Half-and-Half exchange mixing[40] with LYP correlation (BHandHLYP) functionals were utilized. It should be noted that the default Gaussian98 implementation of the BHandHLYP method does not correspond to the original definition by Becke because the HF exchange replaces only the total DF exchange without modifying the DF correlation. Scheme 1 summarizes the applied density functionals and presents their relations to HF theory. The position of the B3LYP method is notable, because this method lacks 28% of the nonlocal DF exchange (ΔE_XB88) and 19% of the nonlocal DF correlation (ΔE_CLYP) as a result of the empirical parametrization ($E_{XC} = E_{XC}$LSDA + $0.72\Delta E_X$B88 + $0.20E_X$-HF − $0.20E_X$LSDA + $0.81\Delta E_C$LYP), and the HF exchange (E_XHF) replaces 20% of the local DF exchange (E_XLSDA) component.

Single point calculations were performed using energy change convergence criterion of less than 10^{-8} a.u. Population analyses were carried out employing Mulliken (MPA),[41] Weinhold's Natural Population Analysis (NPA)[42−44] and Bader's Atoms-in-Molecule (AIM)[45−49] methods. The NPA results are found to be sensitive to the selection of valence orbitals. As suggested by Maseras and Morokuma[50] for transition metals, inclusion of the 4p orbitals into the valence set can have significant influence on the total atomic charges, however, only insignificant effect was observed on the spin densities. It is worth mentioning that the extension of the valence orbitals is critical in obtaining the D_{4h} Lewis structure and natural bonding orbitals.

DFT excitation energies were calculated using three formalisms. The Kohn−Sham orbital energies using GTOs or STOs did not reproduce either the order or the magnitude of the transition energies; therefore, these results are not presented. The calculated excitation energies were significantly improved by ΔSCF-DFT[51] calculations using either type of basis sets. In ADF, all excited-states were obtained, however in Gaussian, certain states collapsed into the ground-state. Time dependent DFT calculations[52−54] were also carried out and excitation energies were obtained for the hybrid methods. At the BP86/BS5 level, convergence could not be achieved, however mixing of minimal (1%) HF exchange (B(1HF)P86/BS5) lead to a rapid convergence. The hybrid DFT results are numerically different from the corresponding ΔSCF calculations, but the relative trends are highly similar and therefore not discussed here. Rather, these trends were used to estimate the missing states for the ΔSCF-DFT calculations.

Stationary point calculations were considered to be converged if both the maximum and the root-mean-square forces and displacements were less than 10^{-4} a.u. mol^{-1}. The PES around stationary structures was further studied by analytical frequency calculations. In the gas-phase calculation, the default redundant coordinates[55−57] were applied. Relaxed potential energy scans were also performed by constraining one or more Cu−Cl bond length at a given value, whereas all the other internal coordinates were optimized. Solution structures were calculated by the Tomasi's reaction field method[58,59] using polarized continuum model (PCM)[60−65] as implemented in Gaussian98. To get a more balanced description of the solvent cavity surfaces, a fine resolution of the surface area was specified (TSARE = 0.4) and in optimizations the Z-matrix coordinates were used with the GDIIS optimizer,[66−68] which was developed for flat potential energy surfaces. The water solvent parameters were used with dielectric constants of $\epsilon = 78.39$. In solid-phase calculations, all of the default redundant coordinates were removed, the Cartesian coordinates of the lattice atoms were fixed and the internal coordinates were redefined for the central $[CuCl_4]^{2-}$ unit as for the gas-phase structure.

The first Cu−Cl bond dissociation energy (BDE) was calculated without correction for the basis-set superposition error (BSSE). As discussed by Frenking,[69] the BSSE is comparable to the basis-set incompletion error with an opposite sign, which results in error cancellation. The relative BDEs are reasonable and they provide insight into the effects of the corrected bonding description.

Energy decomposition analyses were carried out using Ziegler's extended transition state (ETS) method.[70] In ETS, the bonding energy is decomposed into three major components: ΔE_{elstat}, ΔE_{Pauli}, and $\Delta E_{orbital}$. In the case of $[CuCl_4]^{2-}$, the additional fragment preparation energy is not needed because only atomic fragments were used. The term ΔE_{elstat} defines the electrostatic potential energy between the electron densities of the Cu and Cl atoms obtained from the fragment calculation. The ΔE_{Pauli} defines the repulsion of electrons with the same spin among the atomic fragments at the positions of the complex geometry. The $\Delta E_{orbital}$ defines the orbital stabilization energy upon optimization of the electron density.

Selected ab initio calculations were also performed as references. Only methods are employed, where the generation of electron density is available, because our primary calibration quantities are the atomic spin densities. It is worth noting that the QCISD method[71] gives an excellent description of the

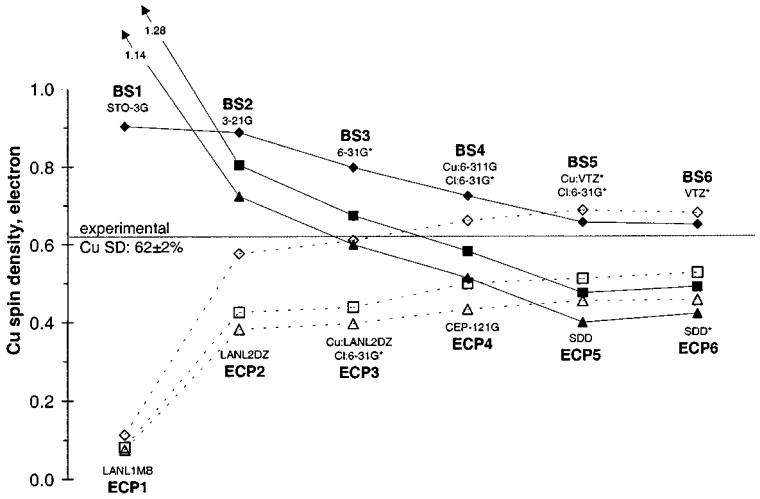

Figure 1. Cu spin densities in D_{4h} $[CuCl_4]^{2-}$ with experimental bond lengths for selected density functionals and basis sets analyzed by Mulliken population analysis. (triangle: BP86, rectangle B3LYP, diamond BHandHLYP; hollow symbol: effective core potential basis set, filled symbol all electron basis set).

ground-state wave function without relativistic correction. Calculations with various Stuttgart/Dresden relativistic pseudopotentials[72−75] did not affect the ground-state spin densities by more than 0.02e.

The hardware used for this study consists of an SGI Origin 2000 8-cpu server, IBM Powerstation 397 workstations, and IBM-compatible PCs equipped with 1 GHz PIII Xeon and 1.4 GHz Athlon processors organized into a 40-cpu heterogeneous cluster.

3. Results and Analysis

3.1. BP86 Ground-State Wave Function. The results for BP86 calculations using various basis sets for the D_{4h} $[CuCl_4]^{2-}$ complex with experimental Cu−Cl bond lengths in the $^2B_{1g}$ ground-state are shown in Figure 1 (triangles). The all-electron and valence orbital basis sets with effective core potentials converge to a Cu atomic spin density of 0.43 ± 0.02e at the basis set saturation limit. The corresponding spin density on each Cl atom is about 0.15e. These values indicate the presence of excessive ligand-to-metal charge transfer in this GGA DFT calculation compared to experiment ($62 \pm 2\%$). The orbital population analysis of the singly occupied HOMO in both spin restricted and unrestricted calculations shows the same behavior as the total atomic spin densities.

Despite the coincidental agreement of the BP86/BS3 results and experiment, the most frequently used double-ζ quality all-electron basis sets are not converged. Rather, the ECP2 valence basis set is a better approximation of the saturation limit. On the basis of the curvature of the spin density plots, at least a triple-ζ quality basis set with diffuse functions (BS5) should be used on the metal in order to achieve effective basis saturation. A larger basis set on the ligand (BS6) does not significantly improve the spin density. The Slater-type numerical basis sets, as implemented in ADF, show better saturation behavior. However, the triple-ζ basis set (BSIV Cu spin density = 0.40e) is required for saturation.

The Mulliken Population Analysis (MPA) results are compared with those obtained from Natural Population Analysis (NPA) and the Atoms in Molecules (AIM) approaches (Table 3). As expected, there are significant differences in the Mulliken partial charges (q) (less for NPA and the least for AIM), however, the spin density remains constant along the series. In NPA, the inclusion of the Cu 4p orbital into the valence orbital set (marked with NPA(4p)), which is normally a Rydberg orbital in the standard NPA, significantly affected the atomic point charges, but only slightly reduced the atomic spin densities. The spin density values increase in the order MPA < NPA < AIM, but deviate from each other by less than 0.07 e (BP86/BS5). In agreement with MPA results, the calculated spin densities from NPA and AIM also lie below the experimentally determined spin density.

TABLE 3: Comparison of Cu Atomic Charges and Atomic Spin Densities Calculated from Different Population Analyses in D_{4h} $[CuCl_4]^{2-}$ for Selected Basis Sets

	atomic partial charges (q)				atomic spin densities (SD)			
method	MPA	NPA	NPA(4p)	AIM	MPA	NPA	NPA(4p)	AIM
BP86/BS3	0.28	1.15	0.63	0.88	0.60	0.62	0.61	0.60
BP86/BS5	0.16	0.96	0.52	0.88	0.40	0.42	0.41	0.47
BP86/ECP2	−0.20	0.85	0.21	0.90	0.39	0.40	0.39	0.45
BP86/ECP5	−0.26	0.83	0.27	0.80	0.45	0.47	0.46	0.51

To further evaluate the copper-ligand bonding description, calculations of excited electronic states were performed using the ΔSCF-DFT formalism. The differences between the computed and experimental[76] excitation energies are presented in Figure 2. In the case of the BP86 set of functionals (triangles in Figure 2), the calculated ligand field transitions are shifted to higher energies and the charge-transfer transitions to lower energies. Not even the order of the excited-states was reproduced, for example, the $^2E_{1g}$ and $^2B_{2g}$ states are reversed. Consistent with the spin densities calculated using different basis sets, the description of the excited-states is improved by saturation of the basis set (e.g., ECP2 and BS5 in Figure 2). Once the saturated limit is reached, further increase of the basis set size does not introduce significant improvement using either Gaussian or Slater-type orbitals.

The above results at BP86 level indicate that the bonding description for the ground-state of D_{4h} $[CuCl_4]^{2-}$ is too covalent (Scheme 2A), which is defined as too much ligand character in the singly occupied HOMO. On the basis of MO theory, this indicates interaction of ligand orbitals with a lower-lying copper d-manifold resulting in a large spin density on the ligand. Consequently, the ligand-field (LF) transitions are shifted to higher and the ligand-to-metal charge transfer (CT) transitions to lower energy relative to the experiment. A less covalent bonding description with increased metal character in the HOMO requires destabilization of the copper d-manifold relative

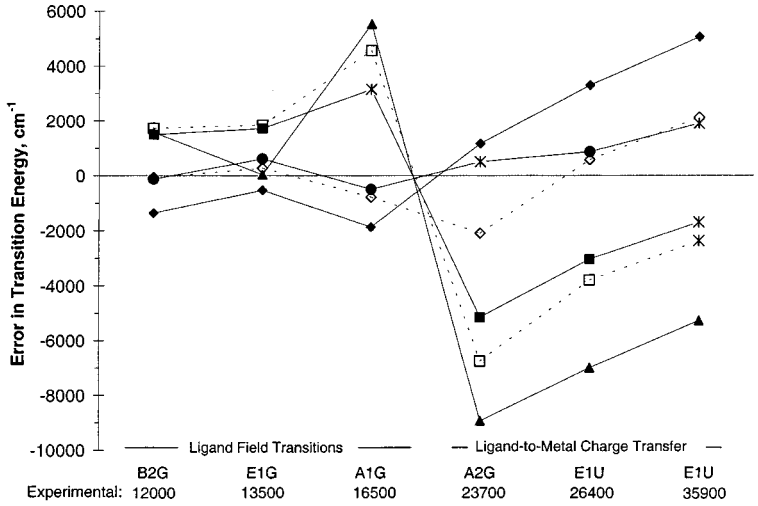

Figure 2. Error plot of calculated LF and CT transitions. (triangle: BP86, rectangle: B3LYP, circle: B(38HF)P86, diamond: BHandHLYP; hollow symbol: effective core potential basis set (ECP2), filled symbol all electron basis set (BS5); star indicates collapse to the ground- or an unintended state).

SCHEME 2: MO Diagram of the Cu−Cl Bond. (A) Inverted Bonding Descriptions (B) Destabilized Copper d-manifold

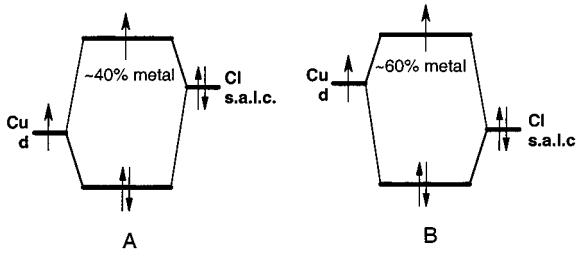

to the ligand orbitals (Scheme 2B). This would increase the spin density on the Cu and shift the CT transitions to higher energies and the LF transitions to lower energies.

3.2. Hybrid DFT Ground-state Wave Functions. By combining density-functional approximations with Hartree−Fock theory, one can make use of the advantages of each method. In our case, mixing ionic HF character into the covalent DFT wave function can destabilize the metal d-manifold and improve the ground-state description. First, the performance of the B3LYP method is examined, and then the mixing of the HF exchange into the DFT exchange functional is optimized based on experimental data.

3.2.1. B3LYP Functionals. As seen in Figure 1 (rectangles), the spin density plots obtained from B3LYP functionals are shifted about 5−10% toward a more ionic description, i.e., larger Cu spin density values relative to BP86. The all electron and effective core potential basis sets converge to a value of 0.55 ± 0.03e for the Cu spin density. This shows an improved ground-state bonding description; however, it is still too covalent compared to the experimental spin density (0.62 ± 0.02e).

The behavior of different population analysis methods parallel those found for the BP86 calculations. The Cu spin densities analyzed by MPA (BS5: 0.48e, ECP5: 0.52e) and AIM (BS5: 0.52e; ECP5: 0.59e) show a deviation of less than 0.07e.

As the spin density values are improved, the transition energies improve relative to experiment (Figure 2). The ligand-field transitions are shifted to lower energies, whereas the charge transfer transitions are shifted to higher energies. The error of the B3LYP method in excitation energies is approximately half of that for the BP86 method. In addition, the order of the excited-states is reproduced, which is not the case at the BP86 level.

The 20% mixing of HF exchange in B3LYP significantly improves the ground and excited-state properties of D_{4h} $[CuCl_4]^{2-}$, but still does not provide the proper bonding description. Extrapolating the effects of going from the BP86 to the B3LYP method, a larger amount of HF mixing is required to obtain the proper bonding description.

3.2.2. Spectroscopic Calibration of Density Functionals. Above, only the different amount of HF exchange was emphasized in the comparison of BP86 and B3LYP functionals. However, the improved bonding description could also originate from their different correlation functionals (P86 compared to LYP). However, calculations show that using BLYP or B3P86 functionals gives virtually identical atomic spin densities to BP86 and B3LYP, respectively. The change due to the different correlation functionals is less than 2% in the Cu spin density (see Section 3.3.3). The improvement in the spin density, therefore, must come from the inclusion of the HF exchange. This assumption is also supported by calculations using Becke's half-and-half functional (Figures 1 and 2, diamonds). The BHandHLYP set of functionals gives a too ionic bonding description (0.67 ± 0.01e). The magnitude of the error in LF and CT transitions is similar to that obtained using the B3LYP method however the sign is opposite. The effects of the different ratios of HF and DFT exchanges strongly indicate that there should be an optimum value between 20% and 50%, which matches the experimental ground-state spin density and excitation energies.

The amount of HF exchange was optimized by systematically varying the local and nonlocal exchange and correlation functionals. The optimization was carried out by comparing the MPA calculated Cu spin density with experiment. Because the optimal value of the HF exchange mixing was only slightly different (deviation is less than 2%) in the different combinations, 38% of the total DF exchange (local and nonlocal) was replaced with HF exchange to match the experimental spin density keeping the DF correlation unchanged ($E_{XC} = 0.62E_X^{LSDA} + 0.62\ \Delta E_X^{B88} + 0.38E_X^{HF} + \Delta E_C^{P86}$). Although the spectroscopic calibration was carried out using the B88 exchange and P86 correlation functionals as implemented in Gaussian98, the amount of HF exchange is transferable to other functionals such as BLYP (vide supra). Using this hybrid functional adjusted to the ground-state, the LF and CT transition

TABLE 4: Results of Geometry Optimizations of D_{4h} and D_{2d} Symmetric $[CuCl_4]^{2-}$ Complexes: Gas-Phase Optimized Cu−Cl Bond Length (d, Å), Distortion from Ideal Tetrahedral Structure (α, °), Calculated Spin Density of the Cu Atom at the Optimized (SD^{opt}, electron) and at the Experimental (SD^{exp}, electron) Structures

	method	d	SD^{opt}	SD^{exp}	φ^a
D_{4h} $[CuCl_4]^{2-}$	BP86/BSIV	2.388	0.41	0.41	
	BP86/BS5	2.361	0.40	0.40	54.7
	B3LYP/BS5	2.368	0.49	0.48	
	B(38HF)P86/BS5	2.330	0.60	0.58	
	BHandHLYP/BS5	2.355	0.70	0.66	
	solid phase experimental[27]	2.264		0.62 ± 0.02	54.7
D_{2d} $[CuCl_4]^{2-}$					
	BP86/BS5	2.340	0.48	0.47	4.3
	B3LYP/BS5	2.347	0.59	0.57	4.3
	B(38HF)P86/BS5	2.314	0.74	0.69	3.8
	BHandHLYP/BS5	2.339	0.83	0.76	3.1
	solid phase experimental[27]	2.209		0.7	4.8

[a] the difference in the half of the smaller Cl−Cu−Cl bond angle and the ideal tetrahedral value (109.47°)

energies were also in excellent agreement with the experiment (rms deviation is less than 1000 cm^{-1}).

3.3. DFT Calculation of Potential Energy Surface Properties. In this section, the influence of the improved bonding description on the potential energy surface (PES) is investigated. These results are important for the extrapolation to properties of experimentally nondetectable intermediates and discussions of reaction pathways.

Given the inherent instability of the planar $[CuCl_4]^{2-}$ structure to distort into a D_{2d} geometry (vide infra), the gas-phase D_{4h} structure was studied initially, which corresponds to a transition state along the b_{2u} distortion mode followed by a less detailed study of the D_{2d} complex. In Section 3.4, we systematically determined that the minimal environment from the crystal structure, which is necessary to stabilize the complex from distortion to a D_{2d} geometry.

3.3.1. Gas-Phase PES Points. Table 4 shows the results of geometry optimizations for the D_{4h} $[CuCl_4]^{2-}$ molecule in the gas phase at different levels of theory.

At standard DFT levels (BP86, B3LYP, and BHandHLYP), the calculated Cu−Cl bond lengths are more than 0.1 Å longer than the experimental values. The spectroscopically calibrated B(38HF)P86 calculation gives a shorter Cu−Cl bond; however, it is still 0.07 Å longer than the experimental value.

The bond length trends among the various DFT functionals are rather different than those for the spin densities and excitation energies. The Slater (BSIV) and Gaussian (BS5) type orbitals using the same set of functionals (BP86) give different optimized Cu−Cl bond lengths (2.388 Å vs 2.361 Å, respectively), although the spin densities in both the experimental and the optimized geometries are virtually identical (Table 4). The optimized Cu−Cl bond lengths at the B3LYP level are slightly longer (2.368 Å) and for BHandHLYP they are slightly shorter (2.355 Å) than at the BP86/BS5 level. The Cu spin densities calculated by the two hybrid methods increase form 0.49e to 0.70e, respectively. The Cu spin density in the optimized geometry of the B(38HF)P86 functionals lies between the B3LYP and BHandHLYP values, however, the Cu−Cl bond (2.330 Å) is the shortest among all the DFT methods. In contrast to the spin densities, there is clearly a nonlinear correlation between the bond length and the amount of HF exchange, which is due to the use of different type and amount of correlation functions (vida infra Sections 3.3.2 and 3.3.3).

To further evaluate the PES of the gas-phase, D_{4h} $[CuCl_4]^{2-}$ molecule, frequency calculations were performed using both

TABLE 5: Calculation of a_{1g} Normal Mode Frequencies ($\nu(a_{1g})$, cm^{-1}), Corresponding Force Constants ($f(a_{1g})$, N m^{-1}) and Imaginary Frequencies (ν_{imag}, cm^{-1}) in D_{4h} $[CuCl_4]^{2-}$ Models

method	ν_{imag}	$\nu(a_{1g})$	$f(a_{1g})$
D_{4h}, gas-phase, experimental geometry			
BP86/BSIV	−79	281	1.6727
BP86/BS5	−77	285	
B3LYP/BS5	−82	294	1.7853
B(38HF)P86/BS5	−75	294	1.7830
BHandHLYP/BS5	−85	304	1.8993
D_{4h}, gas-phase, optimized geometry			
BP86/BSIV	−45	213	1.0645
BP86/BS5	−48	227	
B3LYP/BS5	−51	233	1.1204
B(38HF)P86/BS5	−54	255	1.3444
BHandHLYP/BS5	−57	252	1.3041
solid phase experimental[77]		276	

experimental and optimized geometries (Table 5). Each stationary point had one imaginary, b_{2u} normal mode. The value of the imaginary frequency decreased upon optimization, however, it was not eliminated completely due to the D_{4h} symmetry constraint. This imaginary mode disappeared when the symmetry of the molecule was reduced to D_{2d} (vide infra).

The experimental vibrational value available is that of the total symmetric (a_{1g}) Raman active breathing mode, which is 276 cm^{-1} [77] in the ground-state of D_{4h} $[CuCl_4]^{2-}$. A small influence of the b_{2u} imaginary frequency is expected on the calculated a_{1g} mode mainly due to the small change (0.02 Å) in the calculated Cu−Cl distance upon distortion to D_{2d} geometry (Table 4).

As a consequence of the longer optimized Cu−Cl bonds in these computations, the frequency of the a_{1g} mode in the experimental geometry is overestimated; although, the error is less than 20 cm^{-1}. After optimization, the bond lengths are elongated to such an extent that the Raman active mode becomes underestimated. The longer Cu−Cl bonds decrease both the interaction of the ligands with the Cu atom and the electronic repulsion between the ligands. This makes the curvature of the totally symmetric mode more shallow, which corresponds to lower frequency values. Overall, among the methods presented in Table 5, the spectroscopically calibrated B(38HF)P86 method gives the largest, thus closest to experiment, a_{1g} frequency for the geometry optimized structures. On the basis of the harmonic force constants the strongest Cu−Cl bond is calculated in the B(38HF)P86 method.

To address the effect of various DFT functionals on the bond strength, the potential energy surface of $[CuCl_4]^{2-}$ was also studied at the dissociation limit of the first Cu−Cl bond. Both homolytic and heterolytic bond cleavage were calculated (Figure 3). The homolytic process of the Cu−Cl bond cleavage was calculated to be endothermic at every level of theory. It should be noted that in the homolytic cleavage (i.e., reductive elimination of a Cl atom), the Cu(II) is formally reduced and the resulting Cu(I) complex has a filled d-manifold with a quite different electronic structure than that of Cu(II). One has to be aware that the empirical adjustment for a cupric system might be not directly transferable to a cuprous center. In the heterolytic process, the fragments after dissociation are lower in energy (i.e., more stable) than $[CuCl_4]^{2-}$. This implies that in the gas phase the D_{4h} $[CuCl_4]^{2-}$ molecule would not be stable and environmental interactions are needed to prevent the dissociation.

In gas-phase calculations, presented in Figure 3, the inclusion of HF exchange modifies the dissociation energies by ap-

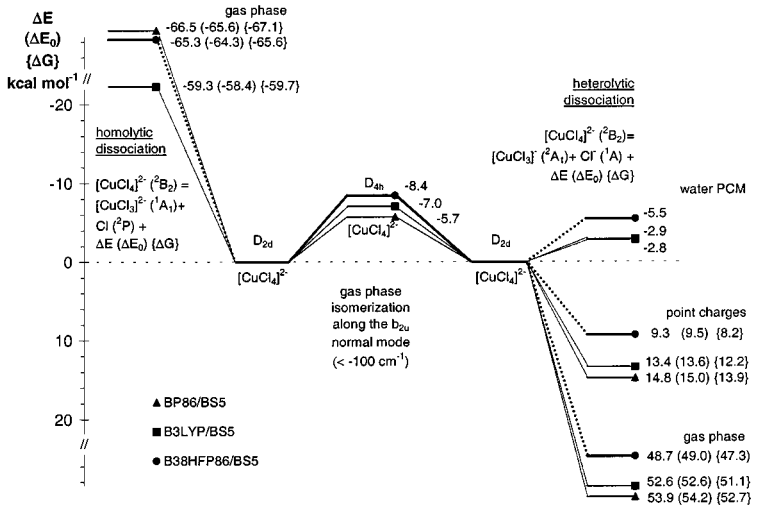

Figure 3. Bond dissociation and isomerization energies of the first Cu−Cl bond in $[CuCl_4]^{2-}$

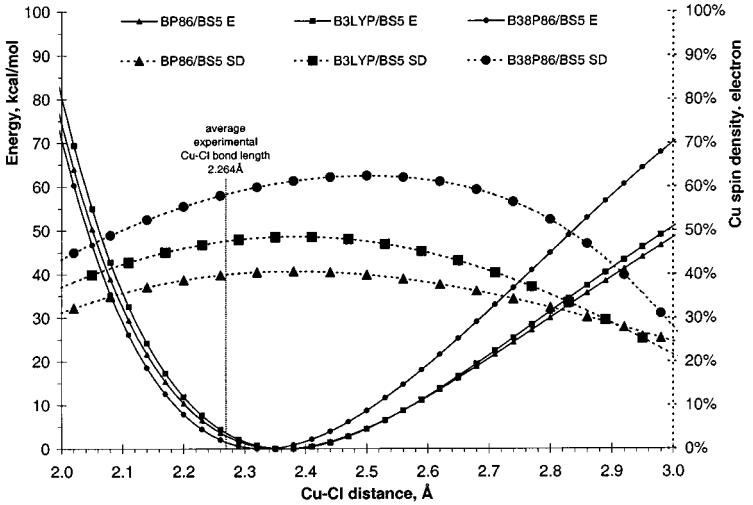

Figure 4. Potential energy and spin density scans of the four Cu−Cl bonds in the D_{4h} $[CuCl_4]^{2-}$ (solid line energy plots, dashed line Cu spin density plots).

proximately 3 to 8 kcal mol^{-1}. In the homolytic process, the bond dissociation energy at the B(38HF)P86 level is between the BP86 and the B3LYP results. On the basis of high level ab initio calculations (vide infra), the GGA approximation seems to give the closest results to the highest ab initio level (QCISD/BS5 $\Delta E = -68$ kcal mol^{-1}) we have studied here. In the heterolytic process, the B(38HF)P86 level gives the smallest, i.e., least exothermic dissociation energy, whereas the B3LYP and the BP86 levels provide about 3.9 and 5.2 kcal mol^{-1} more exothermic ΔE values, which correspond to weaker bonds. The corresponding ab initio dissociation energy is $\Delta E = 47$ kcal mol^{-1}, which is the closest to the B(38HF)P86 result.

3.3.2. Gas-Phase Potential Energy Surface Scans. To gain more insight into the ground-state PES of D_{4h} $[CuCl_4]^{2-}$ beyond the stationary point and the dissociation limit (see Section 3.3.1), potential energy scans were carried out along the a_{1g} normal coordinate. From Figure 4, the amount of HF exchange simultaneously shifts and scales the potential functions (solid lines). The BP86 and B3LYP potential curves look very similar, although the former is shallower as indicated by the lower frequency in Table 5. The difference in the PES minima of the two standard DFT methods is also small as can be seen from the stationary bond lengths in Table 4 (0.007 Å). In contrast, the additional amounts of 18% HF exchange, 19% DF correlation and the different type of correlation in B(38HF)P86 relative to the B3LYP level, shifts the PES to a shorter bond length and forms a steeper parabola (i.e., shorter Cu−Cl bond and larger a_{1g} normal-mode frequency, Tables 4 and 5). A common characteristic of the three functionals is the generally flat potential energy surface. The four Cu−Cl bonds can simultaneously change within approximately 0.1 Å range around the stationary points at the expense of less than 3 kcal mol^{-1}.

The tendencies of Cu spin densities upon scanning the Cu−Cl bond length are also notable (Figure 4, dashed lines). The spin density curves go though a maximum, which is at a longer Cu−Cl distance than the stationary value. At both short and long Cu−Cl distances, the spin density is delocalized mostly over the four Cl atoms. The Cu atom approaches a cuprous state with a fully occupied d-manifold, which can be explained by the high electron affinity of Cu(II) and low ionization potential of Cl^- anion (−21 eV and +3 eV, respectively, at the BP86/BS5 level of theory). The spin density curves are rather flat around the equilibrium geometry, which explains why no significant change is observed in the Cu spin densities upon optimization (0.02e at the B(38HF)P86 level, see Table 4).

3.3.3. Effects of Systematic Variation of Exchange and Correlation Functionals. Figure 5 presents spin densities and optimum Cu−Cl bonds lengths as functions of the systematic replacement of DF exchange with HF exchange (Figure 5A) and the gradual reduction of the DF correlation in the BP86 set

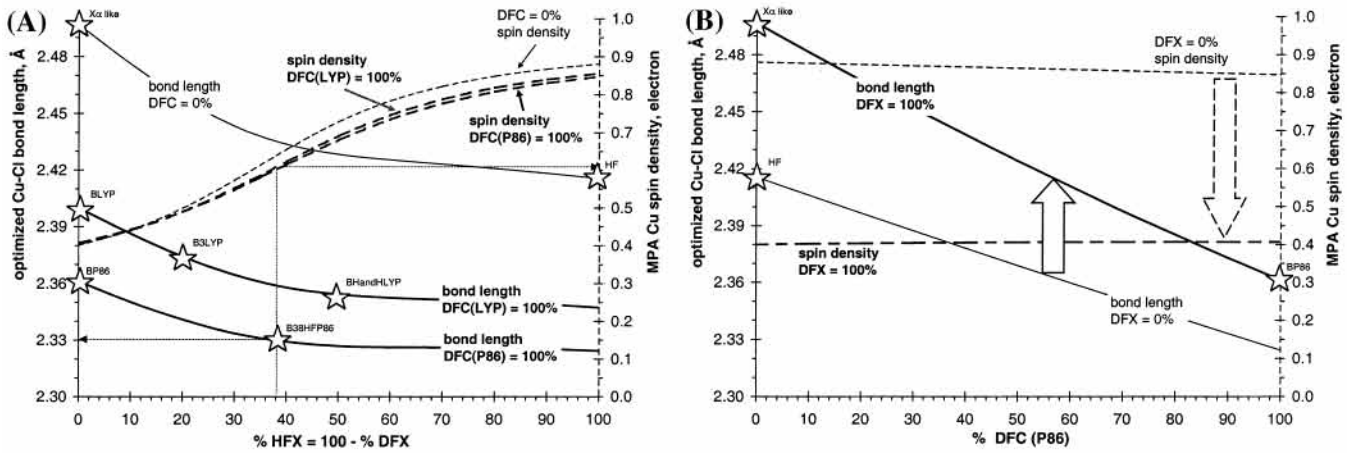

Figure 5. (A) Optimized Cu−Cl bond lengths (Å) and MPA Cu spin densities (electron) in D_{4h} $[CuCl_4]^{2-}$ as function of density functional exchange (DFX: B88) substitution by Hartree−Fock exchange (HFX) at maximal and minimal density functional correlation (DFC: solid black P86; solid gray LYP) limits using BS5. (B) Optimized Cu−Cl bond lengths (Å) and MPA Cu spin densities (electron) in D_{4h} $[CuCl_4]^{2-}$ as function of the amount of density functional correlation (DFC: P86) at maximal and minimal density functional exchange (DFX: B88) limits using BS5.

of functionals toward the HF limit (Figure 5B). These figures demonstrate the sensitivity of the atomic spin densities to the ratio of HF and DF exchanges ($\Delta SD \approx 45\%$) and the small influence of the DF correlation ($\Delta SD < 5\%$) on them. In Figure 5A, the spin density curves nearly asymptotically approach the ionic HF limit (85−87% Cu character).

On the basis of the trends in Figure 5, the optimized Cu−Cl bond lengths are affected by the amount of HF exchange and the type of the DF correlation with an upper limit of 0.04 Å. Alternatively, the total amount of the DF correlation can influence the bond length by up to 0.17 Å. Upon variation of the amount of the HF exchange, the stationary Cu−Cl bond lengths show an asymptotic behavior similar to the atomic spin densities gradually leveling off at approximately 50% HF exchange. The nonsystematic change of bond lengths in comparison of BP86, B3LYP, and B(38HF)P86 can be understood based on Figure 5. The longer Cu−Cl bonds at the B3LYP level partially result from the use of different type and amount of correlation functional, as well as the change in the HF exchange mixing compared with the BP86 based methods. As seen in Figure 5A, the optimized bond lengths using the LYP DF correlation is about 0.04 Å longer than using the P86 functional and this difference is not affected by the amount of HF exchange. Alternatively, the Cu−Cl bond length is strongly dependent on the amount of DF correlation. Deviation from complete (100%) DF correlation, as found in the B3LYP set of functionals (81%), can itself elongate the optimized bond lengths by about 0.02 Å (see Table 4). Within the set of BP86, B3LYP and B(38HF)P86 functionals, which covers 0−38% mixing of HF exchange, 81−100% DF correlation and two different types of correlation functionals (LYP and P86), the overall geometry change in the stationary point is about 0.02−0.04 Å, whereas the spin densities (and other electronic structure properties) are strongly influenced by the amount of HF exchange (by 20% in the case of D_{4h} $[CuCl_4]^{2-}$).

The effect of DF correlation on the geometry can be rationalized by the increased occupation of the LUMO and higher unoccupied orbitals at the expense of HOMO and lower orbital occupations upon incorporation of the dynamical correlation. The low-lying unoccupied orbitals (Cu and Cl 4s, 4p) have less antibonding character than the high-lying occupied orbitals (Cu d manifold combined with Cl p orbitals), and overall, this results in decreased antibonding interaction between the Cu and Cl atoms. The importance of the amount and type of DF correlation supports the replacement of the B88 DF exchange with HF exchange, whereas the P86 DF correlation was left unaltered; otherwise the optimized Cu−Cl bond lengths would have been longer (see Figure 5B).

3.3.4. Energy Decomposition Analyses. The Cu−Cl bond length contracts upon incorporation of HF exchange, which results in a more ionic description. To gain more insight into this bond contraction, simplified energy decomposition analyses (EDA) were carried out for the GGA and hybrid DFT wave functions.

First, calculations of the bonding energy at optimized D_{4h} $[CuCl_4]^{2-}$ geometries were performed using atomic fragments with different effective nuclear charges. The fragment charges were taken from the MPA results of the GGA (BP86), hybrid (BHandHP86) DFT, and HF calculations with complete DF correlation using BS5. The results of the EDA (Table 6) demonstrate that the bonding stabilization increases as the wave function approaches the hypothetical ionic limit of the atomic fragments. Simultaneously, the steric energy (Pauli repulsion and electrostatic attraction) decreases. However, the sum of the nonelectrostatic terms (Pauli repulsion and orbital stabilization) remains quite constant throughout the series. The increase of bonding stabilization can be attributed to the increase in the electrostatic attraction. This observation argues for the dominance of ionic over covalent interactions. On the basis of this simplified EDA scheme, the Cu−Cl bond contraction can be explained by an increasing weight of the ionic character in the bonding.

Focusing only on the electrostatic interactions, a simple point charge model can estimate the change in the ligand−ligand repulsion and metal−ligand attraction upon increasing the amount of HF exchange (see Supporting Information, Figure S2). The total Coulomb interaction energy between the atomic fragments is defined by six (two long and four short) ligand−ligand repulsion and four metal−ligand attraction terms. The atomic point charges were taken from the MPA results as in the EDA−DFT analysis. From Figure S2, it can be seen that the increase of the attraction energy overcomes the increase of repulsion energy, therefore more stabilization is present at the ionic limit relative to the covalent DFT limit. The excess metal−ligand attraction would lead to bond contraction, as observed.

3.4. Environmental Effects on the Potential Energy Surface. The remaining difference between the experimental and best theoretical (B(38HF)P86/BS5) Cu−Cl bond lengths

TABLE 6: Energy Decomposition Analyses (in eV) of D_{4h} $[CuCl_4]^{2-}$ Using Atomic Fragments with Different MPA Charges Obtained from Hybrid DFT Calculations (in stationary point geometries)

fragment charges	charges obtained from	ADF-EDA breakdown		subtotals[a]		bonding energy
$Cu^{+0.24}$ $Cl^{-0.56}$	100% DFX	Pauli:	+21.3			−2.7
	100% DFC	elect.:	−7.1	steric:	+14.2	
		orbit:	−16.9	nonelect.:	+4.4	
$Cu^{+0.48}$ $Cl^{-0.62}$	50% DFX=HFX	Pauli:	+20.4			−3.7
	100% DFC	elect.:	−8.3	steric:	+12.1	
		orbit:	−15.8	nonelect.:	+4.6	
$Cu^{+0.64}$ $Cl^{-0.66}$	100% HFX	Pauli:	+19.7			−4.7
	100% DFC	elect.:	−9.3	steric:	+10.4	
		orbit:	−15.1	nonelect.:	+4.6	
$Cu^{+2.00}$ $Cl^{-1.00}$	theoretical	Pauli:	+11.8			−28.9
	ionic limit	elect.:	−31.9	steric:	−20.1	
		orbit:	−8.8	nonelect.:	+3.0	

[a] Steric = Pauli + Electrostatic; Nonelectrostatic = Pauli + Orbital

(2.264 Å vs 2.330 Å) and the presence of an imaginary b_{2u} mode prompted us to investigate the importance of environmental effects on the structure and to validate the various DFT functionals in solution and solid phases.

All the above computations in gas phase were restricted to D_{4h} symmetry, which resulted in an imaginary frequency for the geometry optimization regardless of the level of theory. In terms of the gas-phase potential energy surface, the D_{4h} stationary point corresponds to a first-order transition state, which connects two (identical) D_{2d} structures through the b_{2u} out-of-plane distortion (Figure 3). Reoptimization of the $[CuCl_4]^{2-}$ complex without a symmetry constrain leads to D_{2d} structures, which are characterized as true minima (Tables 4 and 5).

The accuracy of these optimizations is comparable to those for the D_{4h} geometry. In all cases, the calculated bond lengths in the D_{2d} geometry are longer than the experimental value (2.264 Å). The hybrid method with 38% HF exchange provides better agreement with experiment than the standard DFT methods. The Cu spin densities are also improved using the B(38HF)P86 functionals. Consistent with the D_{4h} $[CuCl_4]^{2-}$ complex, the Cu spin densities in the equilibrium geometries are slightly larger (more ionic bonding) compared to the results of calculations using the experimental structure.

The differences in the energy upon optimization of the D_{4h} to the D_{2d} structure are 5.7, 7.0, 8.4, and 8.5 kcal mol^{-1} for BP86, B3LYP, B(38HF)P86, and BHandHLYP functionals, respectively, using the BS5 basis set (Figure 3).

To obtain a PES, where the D_{4h} $[CuCl_4]^{2-}$ molecule is a true minimum, we extended our study to investigate various solvation models. Further, the crystal structure of $(nmpH)_2[CuCl_4]$ was used to construct the smallest environment, necessary to stabilize the square planar structure.

3.4.1. Solvent Effects. The effect of solvation models on the properties of the ground-state wave function was studied. It was found that, using point charges or continuum models with different dielectric constants, variation of Cu spin density is not more than 2%. The solvation effect of the excitation energies is also less than 1000 cm^{-1}.

Due to the negative charge of the molecule and the charge separation in the heterolytic bond dissociation process, significant solvent effects are anticipated on the PES properties. Therefore, simplified solvated PES studies were carried out using various point charge models, including six orthogonally arranged point charges of +0.333e at 5 Å from the Cl atoms. The polarized continuum model (PCM) with water parameters was also applied.

Regardless of the point charge positions or the magnitude of the dielectric constant, nonnegligible imaginary frequencies (about −100 cm^{-1}) of the b_{2u} mode were observed in all of the D_{4h} geometry optimizations. Once the symmetry of the optimization was reduced, the $[CuCl_4]^{2-}$ unit adjusted its position relative to the orthogonally arranged point charges. In all cases, the $[CuCl_4]^{2-}$ unit rotated out from its experimental position and distortion to a D_{2d} geometry occurred.

As expected, the solvent effects greatly influenced the bond dissociation energies. The exothermicity of the first Cu−Cl heterolytic bond dissociation energy is reduced by 30−40 kcal mol^{-1} in the spherically arranged point charges model compared to the gas-phase value (Figure 3). The maximum difference among the three DFT methods studied remained about 5 kcal mol^{-1} as found in the gas phase with the B(38HF)P86 functionals giving the least exothermic value. Additional structural optimization with the continuum did not significantly change the dissociation energy.

The bond dissociation energies by the more sophisticated PCM solvated models become negative (Figure 3) and the dissociation reaction is endothermic. The dissociation energy at the spectroscopically calibrated B(38HF)P86 level is changed by approximately 3 kcal mol^{-1} relative to the BP86 level giving the most endothermic dissociation. These descriptions correspond to a stronger bond as also seen in Cu−Cl bond lengths, force constants and a_{1g} normal-mode frequency.

3.4.2. Crystal Lattice Effects. The solid-state lattice effects were modeled first by an asymmetric point charge model, where four positive point charges were arranged around the $[CuCl_4]^{2-}$ unit as the closest H atoms of the four ammonium counterions in the experimental crystal structure. These calculations were performed without any geometry constraint. The $[CuCl_4]^{2-}$ unit remained planar but rotated reducing the distance between the Cl atoms and the point charges. The optimized geometry has a Cl−point charge distance of 1.45−1.50 Å compared with the initial experimental Cl−H(N) distance of 2.17−2.63 Å. The Cu−Cl distances are 2.26−2.31 Å. Regardless of this excellent agreement with experimental Cu−Cl bond lengths, the Hessian matrix contained two negative eigenvalues in the lowest energy geometry. In addition, the optimized structure of this model system is chemically irrelevant to the present system since it is rather similar to the $[Cu(HCl)_4]^{2+}$ complex. In agreement with examples from the literature,[26] asymmetrically arranged point charges can prevent the D_{2d} distortion; however, these structures do not correspond to true minima on the potential energy surface in our calculations. Therefore, larger and more realistic molecular models had to be considered.

The simplest model using molecular fragments to simulate crystal lattice effects is composed of four ammonium ions. In constrast to the point charge models, the D_{2d} distortion occurred

TABLE 7: Optimized Minimum and Maximum Values of Cu−Cl Bond Lengths (l, Å), Cl−Cu−Cl Bond Angles (θ, °) and Cl−Cu−Cl···Cl out-of-plane Angles (ω, deg.) and Cu Mulliken Atomic Spin Densities (SD, electron) of the $[CuCl_4]^{2-}$ Complex in Solid State Structure Modeling Using BS5/BS2

method	basis set	l	θ	ω	SD
BP86	ECP2	2.362−2.375	89.16−90.85	−0.3−0.7	0.38
B3LYP	ECP2	2.359−2.370	89.17−90.47	−0.4−0.6	0.43
BHandHLYP	ECP2	2.346−2.350	89.42−90.37	−0.2−0.4	0.60
BP86	BS5/BS2	2.304−2.312	89.50−90.53	−0.5−0.3	0.42
B3LYP	BS5/BS2	2.313−2.319	89.51−90.54	−0.5−0.4	0.50
B(38HF)P86	BS5/BS2	2.288−2.290	89.72−90.45	−0.4−0.2	0.60
B(38HF)LYP	BS5/BS2	2.311−2.314	89.65−90.51	−0.4−0.4	0.61
BHandHLYP	BS5/BS2	2.310−2.312	89.66−90.51	−0.3−0.4	0.68
	experiment	2.248−2.281	90.1−89.9	0.0	0.62 ± 0.02

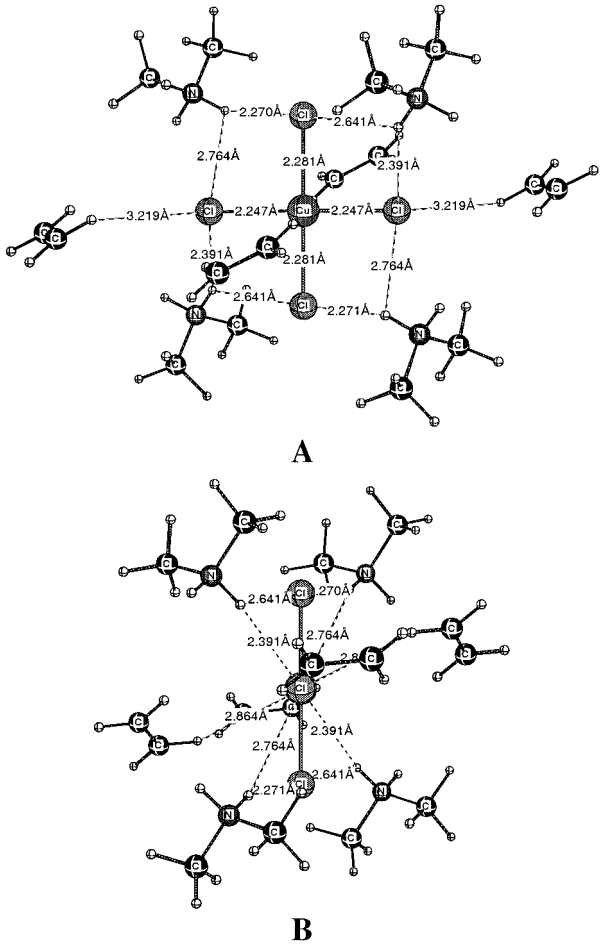

Figure 6. Smallest model of the tetragonal $[CuCl_4]^{2-}$ crystal structure, which prevents the tetrahedral distortion upon geometry optimization (A: top view, B: side view, for optimized coordinates see Supporting Information, p 2).

even when ammonium cations are kept frozen in their experimental positions. The D_{2d} distortion occurred, as well, using the dimethylammonium counterions, although the imaginary frequency the initial experimental geometry decreased in from gas-phase value of 80 cm^{-1} to about 50 cm^{-1}. Employing a finer integration grid and tighter convergence criteria than the default values did not change the outcome of these calculations.

The smallest molecular system, which upon optimization gives a planar Cu complex without any restriction of the $[CuCl_4]^{2-}$ unit, is presented in Figure 6. The model contains four ethylene molecules as the smallest molecular fragments of phenyl groups and four dimethylammonium cations. The fragments were frozen at their experimental positions. The $[CuCl_4]^{2-}$ unit was allowed to geometry optimize freely within the pocket defined by these eight neighboring fragments.

Full optimization at BP86/ECP2 and B3LYP/ECP2 levels gives too long Cu−Cl distances (2.359−2.375 Å). The distortion of the Cl−Cu−Cl angles from 90° and the out-of-plane bending is less than 1°. Using the same basis set, calculation with BHandHLYP functionals gives shorter bond lengths (2.346−2.350 Å), but they are still longer than the experimental value (Table 7). The Cu spin densities of the stationary points (0.38−0.43e) are practically identical to that of the gas-phase structure. As found in the solvent calculations, the solid-state environment of the $[CuCl_4]^{2-}$ unit has no significant effect on the spin densities and consequently on the excitation energies.

To map the PES around the stationary point of the $[CuCl_4]^{2-}$ unit within the solid-phase cavity at the B3LYP/ECP2 level, the four Cu−Cl bonds were compressed to their experimental values ($\Delta l = 0.1$ Å). During the scan, the spin density remained unchanged and the total energy increased by only 4.8 kcal mol^{-1} (about 1 kcal mol^{-1} per Cu−Cl bond). This indicates a quite flat potential energy surface and justifies the need for molecular consideration of environmental effects in order to fine-tune the interactions with the $[CuCl_4]^{2-}$ unit. At the B(38HF)P86/BS5+BS2 level, the binding energy of the $[CuCl_4]^{2-}$ unit within the pocket of the crystal environment is approximately 10 kcal mol^{-1} calculated from the energy difference between the isolated D_{2d} $[CuCl_4]^{2-}$ molecule in its equilibrium geometry and the lattice model in the experimental geometry. This binding energy can be considered as the stabilization energy of the tetragonal structure due to van der Waals and hydrogen bonding interactions originated from the lattice environment.

The effect of basis set saturation on the stationary geometry was studied by using the BS5 basis set for the $[CuCl_4]^{2-}$ unit, and a smaller basis set (BS2) for the environment. In all calculations, the equilibrium geometries were improved and the Cu spin densities were increased compared with the ECP2 results. The Cu−Cl distances are now between 2.304 and 2.319 Å with the standard DFT methods and the $[CuCl_4]^{2-}$ unit stayed planar within 1° deviations (Table 7). Although the Cu−Cl bond lengths are still longer than the experimental values, incorporation of the proper model for the environment successfully prevents the D_{2d} distortion. As seen in the gas phase calculations, improvement for the bond lengths was achieved using the spectroscopically calibrated functional B(38HF)P86, which provided about 0.02 Å shorter Cu−Cl distance, only 0.03 Å longer than the average experimental value. The optimized atomic positions at the B(38HF)P86/BS5+BS2 level of theory are given in the Supporting Information. This is a very good agreement considering the possible improvement of the basis set for the environment. As found for the gas-phase optimizations, use of the P86 DF correlation yields better agreement with experiment than the LYP functional. Interestingly, the 18% additional HF exchange in B(38HF)LYP compared to B3LYP

shortened the Cu−Cl bond lengths by only 0.002−0.005 Å, whereas other geometrical parameters remained unchanged. This finding supports the above results that both the type of correlation functional and the amount of the HF exchange affect the optimized geometry of the $[CuCl_4]^{2-}$ complex.

Results of the solid phase frequency calculations are between the gas phase frequencies calculated at fixed experimental and optimized geometries. The standard BP86 calculation slightly underestimates (261 cm^{-1}), and the spectroscopically calibrated hybrid method overestimates (282 cm^{-1}), the experimental value (276 cm^{-1}).[78]

4. Discussion

Using the D_{4h} $[CuCl_4]^{2-}$ complex to calibrate modern density functional methods, we have found that the GGA DFT methods, such as BP86 and BLYP, generate a bonding description, which is too covalent. The calculated ground-state atomic spin density for the Cu(II) ion is too small (0.40e at the BP86 level using a converged basis set) compared with the experimental value (0.62 ± 0.02e). The calculated charge-transfer energies, which are too low and ligand field transition energies, which are too high, indicate that the metal d-manifold is too stabilized resulting in an inverted bonding description (Scheme 2A). The B3LYP hybrid density functional method improves the bonding by increasing the spin density by approximately 10%, and reducing the error in transition energies by approximately 40%. However, the bonding description in the ground-state is still too covalent.

The inherent self-interaction of the approximate exchange-correlation functionals seems to be responsible for the too covalent bonding description. This excess interaction energy overly stabilizes the d-manifold, thus inverting the bonding description. Self-interaction corrected DFT methods have already been developed and show remarkable improvements in atomic calculations.[38] However, at this time, for molecules they are not as accurate as the GGA or hybrid DFT methods.[79]

The Becke's half-and-half hybrid DFT method gives a description, which is too ionic. This indicates that there is an optimal mixing of HF exchange matching the experimental covalency of the Cu−Cl bond. The amount of HF exchange has been fitted to experiment with the replacement of 38% of the total (local + nonlocal) DF exchange providing a bonding description consistent with experiment. Without further adjustment, we have achieved good agreement of the transition energies (rms error is less than 1000 cm^{-1}), which indicates a reasonable excited-state description, i.e., proper adjustment of the d-manifold energy. We have also found that this experimentally adjusted hybrid density functional (B(38HF)P86) gives a better geometry and improved PES description due to its more ionic bonding description. We have achieved improvement in bond lengths by 0.02−0.03 Å in the $[CuCl_4]^{2-}$ complex. The frequency of the totally symmetric a_{1g} breathing mode of the D_{4h} $[CuCl_4]^{2-}$ complex increases by about 20−30 cm^{-1} and correspondingly the force constant increases by nearly 30% upon inclusion of 38% HF exchange relative to BP86. The stabilization energy of the D_{2d} structure at the B(38HF)P86 level increases by about 3 kcal mol^{-1} compared with the BP86 level. The estimated heterolytic bond dissociation energy of the first Cu−Cl bond in water becomes more endothermic by the same amount.

In addition to the exchange functionals, we have compared the P86 and LYP correlation functionals. The type and the amount of the DF correlation only slightly influence the quality of the ground-state wave function. On the other hand, they both significantly affect the description of the potential energy surface. Gas and solid-phase calculations for the $[CuCl_4]^{2-}$ complex were in better agreement with experiment using the P86 correlation compared to LYP. Substituting part of the DF correlation with HF exchange (as in the B3LYP method, where the nonlocal DF correlation is reduced by 19% as a consequence of the empirical fit) does not significantly alter the ground-state spin density, but elongates the Cu−Cl bonds providing less accurate optimized geometries. The overall effects of variation in the HF exchange and type and amount of DF correlation in the BP86, B3LYP, and B(38HF)P86 functionals on the PES properties are comparable.

TABLE 8: Calculated Mulliken Spin Densities (Cu, electron) of D_{4h} $[CuCl_4]^{2-}$ Complex by ab Initio Methods

	all electron		effective core potentials	
	BS2	BS5	ECP2	ECP5
HF	0.91	0.83	0.81	0.85
MP2	0.83	0.70	0.66	0.70
MP4	0.82	0.67	0.64	0.67
CCD	0.85	0.74	0.68	0.74
CISD	0.86	0.75	0.66	0.74
QCISD	0.78	0.60	0.56	0.58

Becke[80] and Baerends[81] showed that the exchange functionals in modern DFT methods approximate the exact exchange and nondynamical correlation and the correlation functionals approximate the dynamical correlation. It is interesting to compare the effects of correlation in DFT with those in ab initio calculations, where the electron correlation can be systematically included. In the ab initio method, the exact exchange interaction is determined in the Hartree−Fock SCF calculation, which is supplemented with various approximations of dynamical correlation in the post-SCF calculation. The electron density has been generated for the selected methods summarized in Table 8. The Moller−Plesetts perturbation theory[82−86] up to the forth order[87] converges toward a reasonable bonding description, although the highest level of theory employed here (MP4/BS5) still gives an overly ionic description. The coupled-cluster theory (CCD[88,89]) where the electron density is computable gives a poor bonding description because it includes only double substitutions. In the case of the CI approach, the QCISD calculation[71] using the BS5 basis set gives excellent agreement with the experimental spin density and also an improved PES description.[90]

A computational limitation may be the lack of hybrid density functional implementation (e.g., in the ADF package). For such cases, we have employed two alternative approaches: adjustment of the nuclear charge and the introduction of excess effective core potential. These approaches are conceptually similar, but their technical implementations are different. Their performance in electronic structure properties is as good as of the B(38HF)P86; however, their PES descriptions are significantly worse.

In the first approach, the destabilization of the d-manifold energy is achieved by lowering the Cu nuclear charge (Z). As a consequence of the orbital energy shift, the antibonding metal−ligand orbitals gain more metal character. In the simplest implementation, the effect of adjusted Z on the molecular orbitals can be tested using basis sets of atoms with different nuclear charges. By using the BS3 Ni basis set[91] for the Cu atom, the calculated spin density at the B3LYP level decreases by 0.1e matching the experimental value, however at the basis set saturation limit (using BS5 or BSIV) the improvement is less than 0.03e, therefore, basis set modification is not a useful approach for improving the bonding description.

Adjustment of Z can be directly achieved within ADF, where definition of fractional total charges is possible. A Cu atomic fragment with a nuclear charge of 28.55 can match the experimental 62% Cu character of the singly occupied orbital. Beyond the fitting of the antibonding Cu-ligand orbital, the LF and CT transition energies also significantly improve (maximum deviation is about 4000 and 500 cm^{-1}, respectively). On the other hand, the potential energy surface description does not show improvement mainly due to charge imbalance. Upon reduction of the Cu nuclear charge, the electron−electron repulsion becomes more dominant and therefore the optimized Cu−Cl bond lengths are calculated to be very long (2.466 Å).

In the second approach, the implementation of an excess negative potential in the core region can also destabilize the metal d-orbitals and lead to a reasonable bonding description (Scheme 2B). Using the formalism of a well-defined effective core potential (Hay−Wadt[92−94] ECP2), a Gaussian-type external potential was optimized to adjust the spin density on the Cu (see Supporting Information, page 3). The optimized Cu−Cl bond lengths (2.402 Å) are not as long as in the adjusted Z calculations, but significantly longer than for the least accurate standard DFT method.

Overall, the present approach that can be applied for ground and exited state wave functions as well as PES properties is the hybrid DFT method adjusted to experiment. The B(38HF)-P86 method allows a reasonably accurate description of systems with cupric centers. Other metal ions with different oxidation and spin states have to be calibrated as described here. This demonstrates the limitation of the hybrid methods for the correction of self-interaction and a more general correction scheme is required.

The B(38HF)P86 method can be used to study potential energy surfaces of biologically important Cu(II) containing active sites, which is also the focus of our research.[95] In this study, we have found that beyond using an accurate theoretical level, environmental effects are important in determining the proper molecular geometry. The potential energy surface of the $[CuCl_4]^{2-}$ complex around the equilibrium geometry is shallow as also found for the biologically important blue Cu and Cu_A active sites.[96] For the tetragonal geometry, the distortion along the b_{2u} mode is worth 6 to 9 kcal mol^{-1} depending on the DFT functionals used. The potential energy curve along the a_{1g} mode is even more shallow and in the most realistic solid-state model, 0.1 Å change in all four Cu−Cl bonds increases the energy by less than 5 kcal mol^{-1}. It should be emphasized that the tetragonality of the $[CuCl_4]^{2-}$ unit is mostly the result of a proper modeling of the lattice environment.

The entatic state concept[97,98] in bioinorganic chemistry describes the effect of the protein environment on the electronic and geometric structure and reactivity of active sites in metalloproteins. In different systems, the origin, magnitude, and importance of the environment can be different. In the case of the $[CuCl_4]^{2-}$ complex, the gas-phase equilibrium geometry is D_{2d}, thus distorted tetrahedral. In the solid state, the van der Waals component of the steric interactions is one of the contributions to the tetragonal stabilization because the $[CuCl_4]^{2-}$ unit does not interact covalently with its lattice environment. The other important contribution to the D_{4h} stabilization is the extensive hydrogen bonded network with the counterions. These effects are generally considered to be weak interactions, but cannot be dismissed based on their small individual energy contributions to the stabilization, since without them the tetragonal $[CuCl_4]^{2-}$ complex evidently would not exist.

Acknowledgment. This work was supported by the NSF Grant No. CHE9980549. We thank the National Computational Science Alliance CHE990039N for computational time. M.M. thanks the Deutsche Akademische Austausch Dienst for a postdoctoral fellowship.

Supporting Information Available: Coulomb model (Figure S1) of the electrostatic interaction as function of the HF mixing in BP86 functional, optimized coordinates at the B(38HF)P86/BS5+BS2 level of the most realistic solid-state model of the and the definition of an excess negative core potential (Figure S2) adjusting the bonding description of the D_{4h} $[CuCl_4]^{2-}$ are given as Supporting Information. This material is available free of charge via the Internet at http://pubs.acs.org.

References and Notes

(1) Koch, W.; Holthausen, M. C. *A Chemist's Guide to Density Functional Theory*; Wiley-VCH: Weinheim, 2000.
(2) Siegbahn, P. E. M.; Blomberg, M. R. A. *Chem. Rev. (Washington, D. C.)* **2000**, *100*, 421−437.
(3) Eriksson, L. A. *Theoretical Biochemistry: Processes and Properties of Biological Systems*; Elsevier: Amsterdam, 2001; Vol. 9.
(4) Friesner, R. A.; Dunietz, B. D. *Acc. Chem. Res.* **2001**, *34*, 351−358.
(5) Perdew, J. P. *Phys. Rev. B − Cond. Mater.* **1986**, *33*, 8822−8824.
(6) Becke, A. D. *Phys. Rev. A: Gen. Phys.* **1988**, *38*, 3098−3100.
(7) Becke, A. D. *J. Chem. Phys.* **1993**, *98*, 5648−5652.
(8) Kohn, W.; Sham, L. J. *Phys. Rev.* **1965**, *140*, A1133-A1138.
(9) Pople, J. A.; Head-Gordon, M.; Fox, D. J.; Raghavachari, K.; Curtiss, L. A. *J. Chem. Phys.* **1989**, *90*, 5622−5629.
(10) Curtiss, L. A.; Jones, C.; Trucks, G. W.; Raghavachari, K.; Pople, J. A. *J. Chem. Phys.* **1990**, *93*, 2537−2545.
(11) Gewirth, A. A.; Cohen, S. L.; Schugar, H. J.; Solomon, E. I. *Inorg. Chem.* **1987**, *26*, 1133−1146.
(12) Didziulis, S. V.; Cohen, S. L.; Gewirth, A. A.; Solomon, E. I. *J. Am. Chem. Soc.* **1988**, *110*, 250−268.
(13) Solomon, E. I. Bioinorganic Perspectives in Copper Coordination Chemistry. In *Copper Coordination Chemistry: Biochemical & Inorganic Perspectives*; Karlin, K., Zubieta, J., Eds.; Adenine Press: Guilderland, New York, 1982; pp 1−22.
(14) Solomon, E. I.; Gewirth, A. A.; Cohen, S. L. Spectroscopic Studies of Active Sites Blue Copper and Electronic Structural Analogues. In *Excited States and Reactive Intermediates Photochemistry, Photophysics, and Electrochemistry, ACS Symposium Series*; Lever, A. B. P., Ed.; American Chemical Society: Washington, DC, 1986; Vol. 307; pp 236−266.
(15) Solomon, E. I.; Gewirth, A. A.; Cohen, L. S. Recent developments in inorganic spectroscopy. In *Understanding Molecular Properties*; Avery, J., Dahl, J. P., Hansen, A. E., Eds.; D. Reidel Publ. Co.: Dordrecht, 1987; pp 27−68.
(16) Johnson, K. H.; Norman, J. G., Jr.; Connolly, J. W. D. SCF [Self-Consisted-Field]-Xα Scattered-Wave Method. In *Computational Methods for Large Molecules and Localized States in Solids: Proc. Symp.*; Herman, F., McLean, A. D., Nesbet, R. K., Eds.; Plenum: New York, 1973; pp 161−201.
(17) Connolly, J. W. D. *Mod. Theor. Chem.* **1977**, *7*, 105−132.
(18) Roesch, N. The SCF-Xα scettered-wave method with application to molecules and surfaces. In *Electrons in Finite and Infinite Structures*; Phariseau, P., Scheire, J. C., Eds.; Wiley: New York, 1977; Vol. V24; pp 1−143.
(19) Slater, J. C. *The Calculation of Molecular Orbitals*; John Wiley & Sons: New York, 1979.
(20) Penfield, K. W.; Gewirth, A. A.; Solomon, E. I. *J. Am. Chem. Soc.* **1985**, *107*, 4519−4529.
(21) Gewirth, A. A.; Solomon, E. I. *J. Am. Chem. Soc.* **1988**, *110*, 3811−3819.
(22) Becke, A. D. *J. Chem. Phys.* **1992**, *96*, 2155−2160.
(23) Becke, A. D. *J. Chem. Phys.* **1992**, *97*, 9173−9177.
(24) Westbrook, J. D.; Krogh-Jespersen, K. *Int. J. Quantum Chem.: Quantum Chem. Symp.* **1988**, *22*, 245−255.
(25) Waizumi, K.; Masuda, H.; Einaga, H.; Fukushima, N. *Chem. Lett.* **1993**, 1145−1148.
(26) Carloni, P.; Blochl, P. E. *Gaz. Chim. Ital.* **1995**, *125*, 497−500.
(27) Harlow, R. L.; Wells, W. J., III.; Watt, G. W.; Simonsen, S. H. *Inorganic Chemistry* **1974**, *13*, 2106−2111.
(28) Halvorson, K. E.; Patterson, C.; Willett, R. D. *Acta Crystallogr.* **1990**, *B46*, 508−519.
(29) Baerends, E. J.; Ellis, D. E.; Ros, P. *Chem. Phys.* **1973**, *2*, 41−51.

(30) Versluis, L.; Ziegler, T. *J. Chem. Phys.* **1988**, *88*, 322−328.
(31) Te Velde, G.; Baerends, E. J. *J. Comput. Phys.* **1992**, *99*, 84−98.
(32) Guerra, C. F.; Snijders, J. G.; Te Velde, G.; Baerends, E. J. *Theor. Chem. Acc.* **1998**, *99*, 391−403.
(33) Frisch, M. J.; Trucks, G. W.; Schlegel, H. B.; Scuseria, G. E.; Robb, M. A.; Cheeseman, J. R.; Zakrzewski, V. G.; Montgomery, J. A. J.; Stratmann, R. E.; Burant, J. C.; Dapprich, S.; Millam, J. M.; Daniels, A. D.; Kudin, K. N.; Strain, M. C.; Farkas, O.; Tomasi, J.; Barone, V.; Cossi, M.; Cammi, R.; Mennucci, B.; Pomelli, C.; Adamo, C.; Clifford, S.; Ochterski, J.; Petersson, G. A.; Ayala, P. Y.; Cui, Q.; Morokuma, K.; Malick, D. K.; Rabuck, A. D.; Raghavachari, K.; Foresman, J. B.; Cioslowski, J.; Ortiz, J. V.; Stefanov, B. B.; Liu, G.; Liashenko, A.; Piskorz, P.; Komaromi, I.; Gomperts, R.; Martin, R. L.; Fox, D. J.; Keith, T.; Al-Laham, M. A.; Peng, C. Y.; Nanayakkara, A.; Gonzalez, C.; Challacombe, M.; Gill, P. M. W.; Johnson, B.; Chen, W.; Wong, M. W.; Andres, J. L.; Head-Gordon, M.; Replogle, E. S.; Pople, J. A. *Gaussian 98*; *Revision A.1* ed.; Gaussian, Inc.: Pittsburgh, PA, 1998.
(34) Hohenberg, P.; Kohn, W. *Phys. Rev.* **1964**, *136*, B864−B871.
(35) Slater, J. C. *The Self-Consistent Field for Molecules and Solids. Quantum Theory.*; McGraw-Hill: New York, 1974; Vol. 4.
(36) Lee, C.; Yang, W.; Parr, R. G. *Phys. Rev. B: Condens. Matter* **1988**, *37*, 785−789.
(37) Miehlich, B.; Savin, A.; Stoll, H.; Preuss, H. *Chem. Phys. Lett.* **1989**, *157*, 200−206.
(38) Perdew, J. P.; Zunger, A. *Phys. Rev. B: Condens. Matter* **1981**, *23*, 5048−5079.
(39) Vosko, S. H.; Wilk, L.; Nusair, M. *Can. J. Phys.* **1980**, *58*, 1200−11.
(40) Becke, A. D. *J. Chem. Phys.* **1993**, *98*, 5648−5652.
(41) Mulliken, R. S. *J. Chem. Phys.* **1955**, *23*, 1833−1840.
(42) Foster, J. P.; Weinhold, F. *J. Am. Chem. Soc.* **1980**, *102*, 7211−7218.
(43) Carpenter, J. E.; Weinhold, F. *J. Mol. Struct. (THEOCHEM)* **1988**, *169*, 41−62.
(44) Reed, A. E.; Curtiss, L. A.; Weinhold, F. *Chem. Rev.* **1988**, *88*, 899−926.
(45) Bader, R. F. W. *Atoms in Molecules: A Quantum Theory*; Oxford Univeristy Press: Oxford, 1990.
(46) Cioslowski, J.; Mixon, S. T. *J. Am. Chem. Soc.* **1991**, *113*, 4142−4145.
(47) Cioslowski, J.; Nanayakkara, A.; Challacombe, M. *Chem. Phys. Lett.* **1993**, *203*, 137−142.
(48) Cioslowski, J.; Nanayakkara, A. *Chem. Phys. Lett.* **1994**, *219*, 151−154.
(49) Stefanov, B. B.; Cioslowski, J. R. *J. Comput. Chem.* **1995**, *16*, 1394−1404.
(50) Maseras, F.; Morokuma, K. *Chem. Phys. Lett.* **1992**, *195*, 500−504.
(51) Ziegler, T.; Rauk, A.; Baerends, E. J. *Theor. Chim. Acta* **1977**, *43*, 261−271.
(52) Casida, M. E. Time Dependent Density Functional Response Theory for Molecules. In *Recent Advances in Density Functional Theory*; Chong, D. P., Ed.; World Scientific: Singapore, 1995; Vol. 1; pp 1−55.
(53) Gross, E. U. K. Topics in Current Chemistry; TDDFT. In *Density Functional Theory*; Nalewajski, R. F., Ed.; Springer: Heidelberg, 1996.
(54) Stratmann, R. E.; Scuseria, G. E.; Frish, M. J. *J. Chem. Phys.* **1998**, *109*, 8218−8224.
(55) Schlegel, H. B. *J. Comput. Chem.* **1982**, *3*, 214−218.
(56) Schlegel, H. B. In *New Theoretical Concepts for Understanding Organic Reactions*; Bertran, J., Ed.; Kluwer Academic: The Netherlands, 1989; pp 1−33.
(57) Schlegel, H. B. Geometry Optimization on Potential Energy Surfaces. In *Modern Electronic Structure Theory*; Yarkony, D. R., Ed.; World Scientific Publishing: Singapore, 1995.
(58) Miertus, S.; Scrocco, E.; Tomasi, J. *Chem. Phys.* **1981**, *55*, 117−129.
(59) Tomasi, J.; Persico, M. *Chem. Rev.* **1994**, *94*, 2027−2094.
(60) Pascual-Ahuir, J. L.; Silla, E.; Tomasi, J.; Bonaccorsi, R. *J. Comput. Chem.* **1987**, *8*, 778−787.
(61) Floris, F.; Tomasi, J. *J. Comput. Chem.* **1989**, *10*, 616−627.
(62) Cossi, M.; Barone, V.; Cammi, R.; Tomasi, J. *Chem. Phys. Lett.* **1996**, *255*, 327−335.
(63) Cances, E.; Mennucci, B.; Tomasi, J. *J. Chem. Phys.* **1997**, *107*, 3032−3041.
(64) Barone, V.; Cossi, M.; Tomasi, J. *J. Chem. Phys.* **1997**, *107*, 3210−3221.
(65) Barone, V.; Cossi, M.; Tomasi, J. *J. Comput. Chem.* **1998**, *19*, 404−417.
(66) Csaszar, P.; Pulay, P. *J. Mol. Struct. (THEOCHEM)* **1984**, *114*, 31−34.
(67) Farkas, O.; Schlegel, H. B. *J. Chem. Phys.* **1998**, *109*, 7100−7104.
(68) Farkas, O.; Schlegel, H. B. *J. Chem. Phys.* **1999**, *111*, 10806−10814.
(69) Frenking, G.; Antes, I.; Bohme, M.; Dapprich, S.; Ehlers, A. W.; Jonas, V.; Neuhaus, A.; Otto, M.; Stegman, R.; Veldkamp, A.; Vyboishchikov, S. F. Pseudopontential Calculation of Transition Metal compounds: Scope and Limitations. In *Reviews in Computational Chemistry*; Lipkowitz, K. B., Boyd, D. B., Eds.; VCH Publishers: New York, 1996; Vol. 8; pp 63−140.
(70) Ziegler, T. A general energy decomposition scheme for the study of metal−ligand interactions in complexes, clusters and solids. In *Metal−Ligand Interactions: from Atoms, to Clusters, to Surfaces*; Salahub, D. R., Russo, N., Eds.; Kluwer Academic Publishers: Amsterdam, 1992; pp 367−396.
(71) Pople, J. A.; Head-Gordon, M.; Raghavachari, K. *J. Chem. Phys.* **1987**, *87*, 5968−5975.
(72) Fuentealba, P.; Stoll, H.; Szentpaly, L. v.; Schwerdtfeger, P.; Preuss, H. *J. Phys. B* **1983**, *16*, L323−L328.
(73) Dolg, M.; Wedig, U.; Stoll, H.; Preuss, H. *J. Chem. Phys.* **1987**, *86*, 866−872.
(74) Igel-Mann, G.; Stoll, H.; Preuss, H. *Mol. Phys.* **1988**, *65*, 1321−1328.
(75) Bergner, A. D., Michael; Kuechle, Wolfgang; Stoll, Hermann; Preuss, Heinzwerner. *Mol. Phys.* **1993**, *80*, 1431−41.
(76) Solomon, E. I. Inorganic Spectroscopy, An Overview. In *Comments on Inorganic Chemistry*; Sutin, N., Ed.; Gordon and Breach: New York, 1984; Vol. III.; pp 225−320.
(77) Hitchman, M. A. C., P. J. *Inorg. Chem.* **1979**, *18*, 1745−54.
(78) The stationary point at B(38HF)P86/BS5 level gives numerous imaginary frequencies corresponding to rotation and/or translation of the frozen fragment molecules of the lattice environment. The three imaginary modes between −5 and −15 cm^{-1} show slight b_{2u}-type distortion of the $[CuCl_4]^{2-}$ unit, however, no spontaneous D_{2d} distortion was observed during the optimization.
(79) Goedecker, S.; Umrigar, C. J. *Phys. Rev. A: At., Mol., Opt. Phys.* **1997**, *55*, 1765−1771.
(80) Becke, A. D. Exchange-Correlation Approximations in Density-Functional Theory. In *Modern Electronic Structure Theory, Part II*; Yarkony, D. R., Ed.; World Scientific: Singapore, 1995.
(81) Gritsenko, O. V.; Schipper, P. R. T.; Baerends, E. J. *J. Chem. Phys.* **1997**, *107*, 5007−5015.
(82) Head-Gordon, M.; Pople, J. A.; Frisch, M. J. *Chem. Phys. Lett.* **1988**, *153*, 503−506.
(83) Saebo, S.; Almlof, J. *Chem. Phys. Lett.* **1989**, *154*, 83−89.
(84) Frisch, M. J.; Head-Gordon, M.; Pople, J. A. *Chem. Phys. Lett.* **1990**, *166*, 275−280.
(85) Frisch, M. J.; Head-Gordon, M.; Pople, J. A. *Chem. Phys. Lett.* **1990**, *166*, 281−289.
(86) Head-Gordon, M.; Head-Gordon, T. *Chem. Phys. Lett.* **1994**, *220*, 122.
(87) Krishnan, R.; Pople, J. A. *Int. J. Quantum. Chem.* **1978**, *14*, 91−100.
(88) Pople, J. A.; Krishnan, R.; Schlegel, H. B.; Binkley, J. S. *Int. J. Quantum Chem.* **1978**, *14*, 545−560.
(89) Bartlett, R. J.; Purvis, G. D. *Int. J. Quantum Chem.* **1978**, *14*, 516−581.
(90) At the QCISD/BS5 level, the LF transitions are reproduced with a maximum deviation of 1300 cm^{-1}. The LMCT transitions are significantly overestimated ($^2A_{2g}$ ∼2000 cm^{-1}, $^2E_{u1}$ σ and π ∼4000 and 8000 cm^{-1}, respectively). This inaccuracy is probably due to the multireference nature of the LMCT exited states. Optimized gas-phase geometry of the D_{4h} $[CuCl_4]^{2-}$ at QCISD/BS5 level has the shortest Cu−Cl bond length (2.313 Å) and manual optimizations at the QCISD(T)/BS5 shortens the bond length only by 0.01 Å. By taking the these numbers as the best estimate of the gas phase experimental value, the B38HFP86 method gives only 0.03 Å longer bond lengths for both tetragonal and tetrahedral $[CuCl_4]^{2-}$ resulting in the most accurate DFT method.
(91) Rassolov, V. A.; Pople, J. A.; Ratner, M. A.; Windus, T. L. *J. Chem. Phys.* **1998**, *109*, 1223−1229.
(92) Hay, P. J.; Wadt, W. R. *J. Chem. Phys.* **1985**, *82*, 270−83.
(93) Wadt, W. R.; Hay, P. J. *J. Chem. Phys.* **1985**, *82*, 284−98.
(94) Hay, P. J.; Wadt, W. R. *J. Chem. Phys.* **1985**, *82*, 299−310.
(95) Szilagyi, R. K.; Solomon, E. I. *Curr. Opinion in Chem. Biol.* **2002**, *6*, in press.
(96) Ryde, U.; Olsson, M. H. M.; Pierloot, K. *Theor. Comput. Chem.* **2001**, *9*, 1−55.
(97) Gray, H. B.; Malmstreom, B. G. *Comments Inorg. Chem.* **1983**, *2*, 203−209.
(98) Williams, R. J. P. *Eur. J. Biochem.* **1995**, *234*, 363−381.
(99) Collins, J. B.; Schleyer, P. v. R.; Binkley, J. S.; Pople, J. A. *J. Chem. Phys.* **1976**, *64*, 5142−51.
(100) Pietro, W. J.; Francl, M. M.; Hehre, W. J.; Defrees, D. J.; Pople, A. J.; Binkley, J. S. *J. Am. Chem. Soc.* **1982**, *104*, 5039−48.
(101) Dobbs, K. D.; Hehre, W. J. *J. Comput. Chem.* **1987**, *8*, 880−93.
(102) Hehre, W. J.; Random, L.; Schleyer, P. v. R.; Pople, J. A. *Ab Initio Molecular Orbital Theory*; Wiley: New York, 1986.

(103) McGrath, M. P.; Radom, L. *J. Chem. Phys.* **1991**, *94*, 511−516.
(104) Curtiss, L. A.; McGrath, M. P.; Blaudeau, J.-P.; Davis, N. E.; Binning, R. C. J.; Radom, L. *J. Chem. Phys.* **1995**, *103*, 6104−6113.
(105) Schaefer, A.; Horn, H.; Ahlrichs, R. *J. Chem. Phys.* **1992**, *97*, 2571−2577.
(106) Schaefer, A.; Huber, C.; Ahlrichs, R. *J. Chem. Phys.* **1994**, *100*, 5829−5835.
(107) NV, S. C. M. Amsterdam Density Functional; 01 ed.; Vrije Universiteit: Amsterdam, 2000.
(108) Stevens, W. J.; Basch, H.; Krauss, M. *J. Chem. Phys.* **1984**, *81*, 6026−6033.
(109) Stevens, W. J.; Krauss, M.; Basch, H.; Jasien, P. G. *Can. J. Chem.* **1992**, *70*, 612−630.
(110) Stoll, H.; Fuentealba, P.; Schwerdtfeger, P.; Flad, J. *J. Chem. Phys.* **1984**, *81*, 2732−2736.
(111) Wedig, U.; Dolg, M.; Stoll, H.; Preuss, H. Energy-adjusted pseudopotentials for transition-metal elements. In *Quantum Chemistry: The Challenge of Transition Metals and Coordination Chemistry*; Veillard, A., Ed.; D Reidel Publ. Co., Dordrecht: The Netherlands, 1986; Vol. 176; pp 79−89.
(112) Dolg, M.; Wedig, U.; Stoll, H.; Preuss, H. *J. Chem. Phys.* **1987**, *86*, 866−872.